Journal of Cleaner Production 361 (2022) 132278

Contents lists available at ScienceDirect

Journal of Cleaner Production

journal homepage: www.elsevier.com/locate/jclepro

Brake wear induced PM_{10} emissions during the world harmonised light-duty vehicle test procedure-brake cycle

Ye Liu [a,1], Sijin Wu [a,1], Haibo Chen [a,*], Matteo Federici [b], Guido Perricone [b], Ying Li [c], Gang Lv [d,**], Said Munir [a], Zhiwen Luo [e], Baohua Mao [f]

[a] Institute for Transport Studies, University of Leeds, Leeds, LS2 9JT, UK
[b] Brembo S.p.A., Via Europa 2, 24020, Stezzano, BG, Italy
[c] Dynnoteq, 61 Bridge Street, Kington, HR5 3DJ, UK
[d] State Key Laboratory of Engines, Tianjin University, Tianjin, 300072, China
[e] School of the Built Environment, University of Reading, Reading, RG6 6AW, UK
[f] Integrated Transport Research Center of China, Beijing Jiaotong University, Beijing, 100044, China

ARTICLE INFO

Handling Editor: Zhifu Mi

Keywords:
Non-exhaust emissions
Brake wear PM_{10} emissions
WLTP-B cycle
FEA
Machine learning

ABSTRACT

In this work, the particulate matter less than 10 μm (PM_{10}) emissions from a medium-sized passenger vehicle's front brake wear were studied using a finite element analysis (FEA) and experimental approaches. The world harmonised light-duty vehicle test procedure-brake (WLTP-B) cycle was chosen to simulate real-world driving. An electrical low-pressure impactor (ELPI+) was used to count the brake wear particles on a brake dynamometer sealed in a chamber. In addition, a machine learning method, namely, extreme gradient boosting (XGBoost), was employed to capture the feature importance rankings of braking conditions contributing to brake wear PM_{10} emissions. The simulated PM_{10} emissions were quite consistent with the measured ones, with an overall relative error of 9%, indicating that the proposed simulation approach is promising to predict brake wear PM_{10} during the WLTP-B cycle. The simulated and experimental PM_{10} emission factors during the WLTP-B cycle were 6.4 mg km^{-1} veh^{-1} and 7.0 mg km^{-1} veh^{-1}, respectively. Among the 10 trips of the WLTP-B cycle, the measured PM_{10} of trip #10 was the largest contributor, accounting for 49% of total PM_{10} emissions. On the other hand, the XGBoost results revealed that the top five most important factors governing brake wear PM_{10} emissions were dissipation energy, initial braking speed, final rotor temperature, braking power, and deceleration rate. From the perspective of friendly driving behaviour and regulation, limiting severe braking and high-speed braking has the potential to reduce PM_{10} emissions from brake wear.

1. Introduction

Particulate matter (PM) has detrimental effects on not only human health but also visibility and climate change (Fan et al., 2018; Kim et al., 2015; Woo et al., 2021). Exhaust and non-exhaust PM from traffic are considered to be the main sources of PM in urban areas (Grigoratos and Martini, 2015; Oroumiyeh and Zhu, 2021). Exhaust PM is generated as a consequence of the incomplete combustion of fuel and the volatilisation of lubricants, whereas non-exhaust PM is generated as a result of brake wear, tyre wear, road wear, and road dust resuspension (Chen et al., 2020; Liu et al., 2022; Rodovalho and de Tomi, 2017). To meet the increasingly stringent emission regulations, the majority of research has put the spotlight on engine exhaust PM emissions. As a result, great progress has been made regarding engine combustion and after-treatment technologies, significantly reducing exhaust PM emissions. However, the non-exhaust PM emissions from brake wear, tyre wear, and road wear are gradually increasing due to the increased vehicle weight and absence of regulatory restrictions (OECD, 2020). Recent investigations have shown that non-exhaust emissions associated with traffic are comparable to or even more than the PM_{10} from engine pipelines (Amato, 2018; Beddows and Harrison, 2021; Liu et al., 2021).

Among these non-exhaust emissions, PM_{10} from brake wear is a

* Corresponding author.
** Corresponding author.
E-mail addresses: H.Chen@its.leeds.ac.uk (H. Chen), Lvg@tju.edu.cn (G. Lv).
[1] These authors contributed equally to this work.

https://doi.org/10.1016/j.jclepro.2022.132278
Received 16 January 2022; Received in revised form 25 April 2022; Accepted 15 May 2022
Available online 18 May 2022

significant source of non-exhaust emissions. For instance, Gasser et al. (2009) and Lawrence et al. (2013) reported that brake wear PM_{10} accounted for 21% of the PM_{10} emitted from road transport. According to the European Environment Agency (EEA), 34% of the traffic-related PM_{10} was caused by brake and tyre wear (EEA, 2018). Harrison et al. (2012) stated that brake wear particles (BWPs) contributed up to 55% by mass of non-exhaust PM_{10} near a major road in London. In addition, BWPs contain a variety of metal components that are potentially harmful to human health (Amato et al., 2014; Grigoratos and Martini, 2015). Thus, further research is required to better understand the generation mechanism of BWPs, which will aid in developing the control strategy.

Previously, BWPs were analysed mainly using a variety of test-driving cycles initially devised to measure vehicle exhaust gas emissions. For instance, Park et al. (2021) measured the BWPs on a brake dynamometer under the worldwide harmonised light vehicle test procedure. Zum Hagen et al. (2019) and Hagino et al. (2016) measured BWPs under the Los Angeles city traffic driving cycle and Japanese urban driving cycle on a brake dynamometer, respectively. Riva et al. (2019) computed BWPs during the Los Angeles city traffic driving cycle using a finite element analysis (FEA) approach. To the best of our knowledge, however, limited studies were conducted regarding BWPs under the world harmonised light-duty vehicle test procedure-brake (WLTP-B) cycle. The United Nations Economic Commission for Europe has recommended the WLTP-B cycle, developed by Mathissen et al. (2018), as a standard driving cycle for measuring BWPs (Woo et al., 2021). As a consequence, it is necessary to determine the difference in BWPs between the existing driving cycles and the newly developed WLTP-B cycle. In this context, BWPs were investigated using both FEA and experimental approaches under the WLTP-B cycle. The purpose of the simulation approach is to better understand what is occurring at the pad-to-rotor contact during each braking and to compute brake wear PM_{10} emissions. Furthermore, a machine learning method, namely, extreme gradient boosting (XGBoost), was introduced for the first time to explore the effect of braking conditions on BWPs.

2. Simulation and experimental methods

2.1. Brake cases

The WLTP-B cycle was chosen as the test cycle, which was developed based on an investigation of 700,000 driving data points gathered from the European Union, the United States, India, Japan, and Korea. Fig. 1 shows the vehicle velocity profile of the WLTP-B cycle. This cycle takes 4 h 24 min, covers a distance of 192 km and consists of 303 braking events divided into 10 trips. The braking deceleration rates for 303 braking events are in the range of 0.49–2.18 m/s^2, and the average braking deceleration rate is 0.97 m/s^2. The average braking velocity is 43.7 km/h, and the initial braking temperature varies from 40 °C to 175 °C. More detailed information regarding each braking event is given in the Supplemental Material.

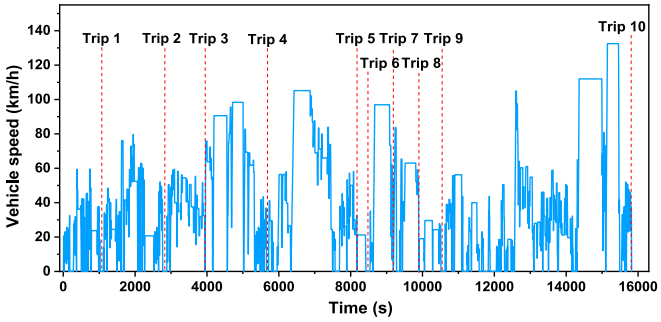

Fig. 1. Vehicle velocity profile during WLTP-B cycle.

2.2. Simulation methodology

Fig. 2 shows an overview of the proposed simulation methodology. First, preprocessing operation consists of creating a three-dimensional model, defining the material properties of different components and setting the driving conditions. Thereafter, tribometer tests were run to obtain the local particle rate with respect to normal contact pressure and sliding velocity (*pv*-map) (Wahlström et al., 2017). This *pv*-map was utilised as input data for the simulation of brake wear emissions. In parallel, the brake wear emissions for each braking event of the WLTP-B cycle were measured on a brake dynamometer. Finally, the experimental results were compared to the FEA ones after post-processing operations. A more detailed explanation will be given in the following sub-sections.

2.2.1. Disc brake system

Fig. 3 illustrates the whole disc brake system, consisting mainly of a floating calliper and a grey cast iron rotor. The floating calliper includes mainly two low-metallic pads, a calliper body, a carrier, a piston, and two sliding pins. The internal and external radius for the disc braking ring are 80 mm and 139 mm, respectively. The pad area is 5080 mm^2 and the cylinder diameter is 57 mm.

2.2.2. Finite element analysis

The FEA was carried out using the commercial software ABAQUS (Abaqus). Fig. 4 shows the meshed components of the disc brake system. The carrier, calliper, and piston head were constructed using a parabolic tetrahedral mesh, whilst the other components were constructed using a linear hexahedral mesh. The size of the mesh was in the range of 2–8 mm, and the average size was 4 mm. The system pressure was applied to the piston head and cylinder walls, and the rotational velocity was applied to the disc. The applied pressure and the rotational velocity were set based on each braking event of the WLTP-B cycle.

For each braking event during the WLTP-B cycle, a quasi-static FEA analysis was carried out to calculate the contact pressure and slip rate of every node and element between the disc and pads at every step of the

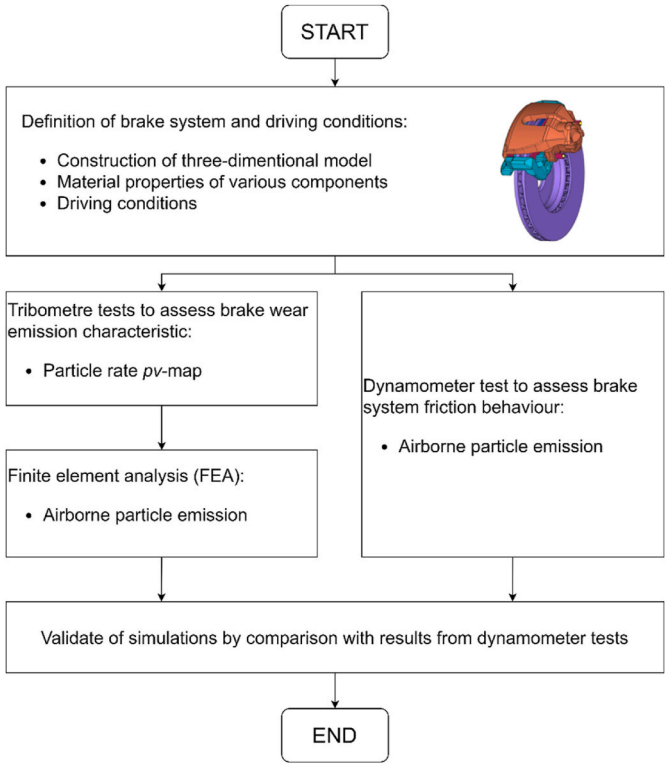

Fig. 2. An overview of the simulated approach.

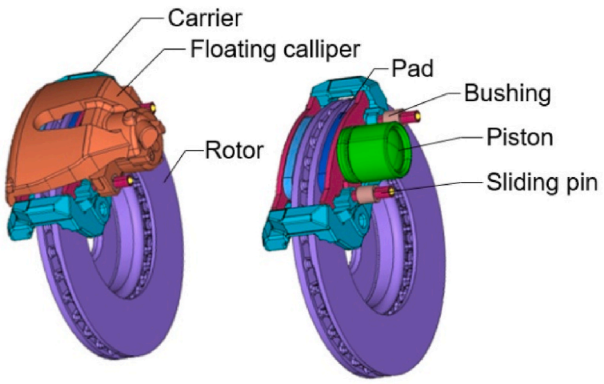

Fig. 3. Single piston disc brake system.

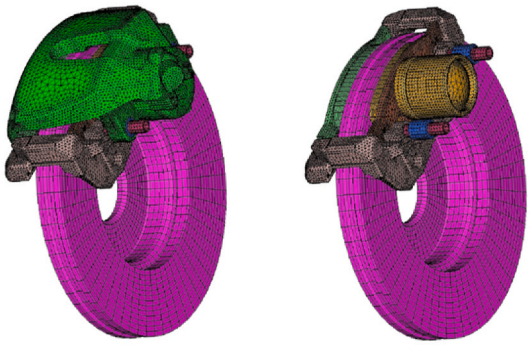

Fig. 4. Meshed components of the disc brake system.

braking. Abaqus Arbitrary Lagrangian-Eulerian adaptive meshing technique was used to update the node positions after every step of each braking event (Abaqus). The slip rate is directly proportional to the rotor rotation velocity. As a result, the larger the radii of the disc, the higher the slip rate, and the slip rate decreases gradually during each braking event.

2.2.3. PM_{10} emission computation

Fig. 5 presents the *pv*-map of airborne particle mass rate that was obtained by our partner's previous work in the pin-on-disc experiments (Wahlström et al., 2017). The pin and disc of the brake system were made, respectively, from low-metallic pads and a grey cast iron. The diameters of the cylindrical pin and disc are 10 mm and 60 mm, respectively. In the pin-on-disc experiments, nominal contact pressure was in the range of 0.3–1.2 MPa, and sliding velocity ranged from 1 m/s to 4 m/s, corresponding to the calliper pressure between 0.6 MPa and 2.4 MPa.

The *pv*-map was used as an input for the FEA to calculate the particle emission. From this map, the particle emissions per sliding distance (μg/m) can be obtained when the sliding velocity and contact pressure of notes are known. As a result, the brake wear mass emission for each brake can be derived from the following equation (Riva et al., 2019):

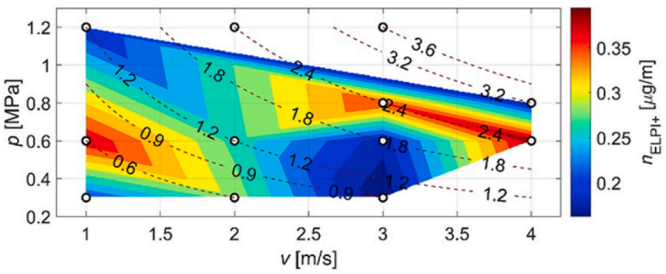

Fig. 5. The mass rate map of the airborne particle (n_{ELPI+}) with respect to normal contact pressure (p) and sliding velocity (v).

$$m_{particle} = \varphi_{POD} \cdot n_{ELPI+(p,v)} \frac{A_{nodal}}{A_{pin}} \quad (1)$$

Where:

- n_{ELPI+} is the mass rate of particle emission obtained from *pv*-map;
- A_{nodal} is the area composed of several nodes in the brake pad (the smallest element);
- A_{pin} is the pin area;
- φ_{POD} is the sampling efficiency during the experiment on pin-on-disc.

The simulation analysis was performed using computational fluid dynamics to obtain a sampling efficiency of 80.1% for PM_{10} emissions in the pin-on-disc experiment (Riva et al., 2017). Given that the contact pressure and deceleration rate were assumed to be constant during every braking event, each braking was able to be time-divided into n sub-steps, as presented in the following equation:

$$m_{particle} = \varphi_{POD} \left(\sum_{i=1}^{n} n_{ELPI+(p,v)} \cdot \Delta s_i \right) \frac{A_{nodal}}{A_{pin}} \quad (2)$$

where ns_i is the sliding distance during a sub-step, which can be calculated using the following linear motion equation, and constant deceleration was assumed.

$$\Delta s_i = v_i \Delta t + \frac{1}{2} a \Delta t^2 \quad 3$$

2.3. Brake dynamometer

The experimental setup is shown in Fig. 6, which includes the brake dynamometer, wind tunnel, and the measuring instrument for brake wear emissions. This rotational weight mimicked a moment of inertia of 49.3 kg m^2, which was equal to the curb weight of the vehicle plus 1.5 passengers and with an assumed brake force distribution of 60% on the front axle. Moreover, the inertia was reduced by 13% with respect to its nominal value of 56.7 kg m^2 to take into account the vehicle parasitic losses. A thermocouple was implanted at a depth of 0.5 mm in the disc to detect the temperature. The entire brake system was sealed inside an oval chamber. To keep the oval chamber particle-free, clean air was provided using a high-efficiency particle air filter (HEPA H13). The air mixed with brake wear particles escaped from the oval chamber into a wind tunnel with a length of 3.5 m and a diameter of 150 mm. A sampling probe was mounted in the wind tunnel. The particle counter with an electric low-pressure impactor (ELPI+) at a flow rate of 10 L/min was used to monitor particle emission within the range of 0.004–10 μm. The brake wear mass per stop was calculated directly from the particle size and numbers, assuming spherical particles:

$$m_i = \left(\sum_{j=d_1}^{j=d_n} N_j \rho V_j \right)_i \quad (4)$$

where m_i is the brake wear mass of the #i braking event, N_j is the number of particles per braking event which have the size d_j, ρ is density that was supposed to be 1 g/cm^3 (Riva et al., 2019), and V_j is the volume of particles that have the size d_j, assumed to be spherical. Prior to measuring brake emissions, a run-in process of 350 brake applications was performed to burnish the brake system surfaces. After the burnishing process, the brake wear test was performed to obtain reliable results (Park et al., 2021; Zum Hagen et al., 2019). The brake wear tests on the brake dynamometer were repeated twice, and the maximum and average deviations of the obtained PM_{10} emissions were found to be at around 27% and 15% during the WLTP-B cycle, respectively.

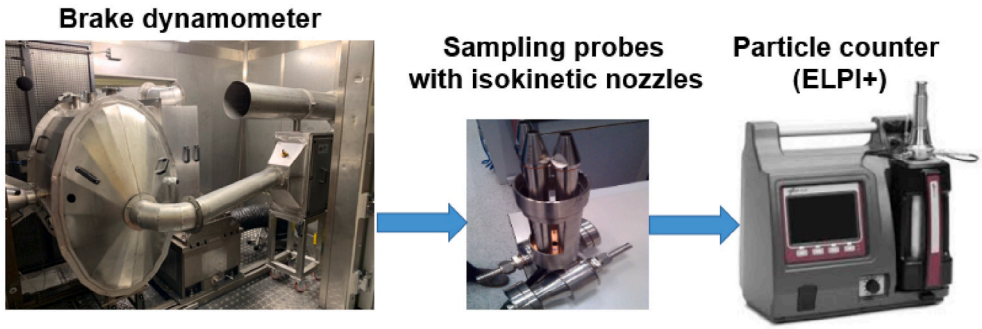

Fig. 6. Brake dynamometer enclosed in a chamber and a device for measuring particles.

2.4. Machine learning model

A machine learning model (XGBoost) was used to capture non-linear correlations between brake wear PM_{10} and braking conditions. The XGBoost model is an ensemble tree-based machine learning algorithm that can exhibit better performance since it is improved and optimised on the basis of the gradient boosting model (Xu et al., 2020). This model primarily consists of three parts, as presented in Fig. 7. In the first part, the data collected from experiments was preprocessed and then feature extraction regarding braking conditions was performed. The model optimisation and cross-validation using GridSearchCV (Ahmad et al., 2022; Pedregosa et al., 2011) were then performed to increase the model accuracy and prevent overfitting after preprocessing of collected data and feature extraction. The determined parameters for the most optimised model are summarised in Table 1. Subsequently, on the basis of the optimised XGBoost model, the importance of braking conditions affecting PM_{10} was identified.

Table 1
The determined parameters of the most optimised model.

Crucial parameters	Value
Learning rate	0.2
Min child weight	3
Sample subsampling rate	0.4
Maximum tree depth	3
L1 Regular Coefficient	0.08
L2 Regular Coefficient	1

3. Results and discussion

3.1. Brake wear simulation

Fig. 8 shows two examples (braking events #22 and #299) regarding the contact pressure distribution of both piston and finger sides from FEA analysis. The pressures in the cylinder of the calliper for these two braking events were 0.39 MPa and 0.44 MPa, respectively. The output simulation contour plots refer to the end of both the braking events. It can be observed that the contact pressure contours for both the braking events were quite similar. The contact pressure of the piston pad presented an increase towards the disc inner side, which had a transversal gradient from outer to inner side. On the finger side, the contact pressure distribution showed a gradient from small to large radii.

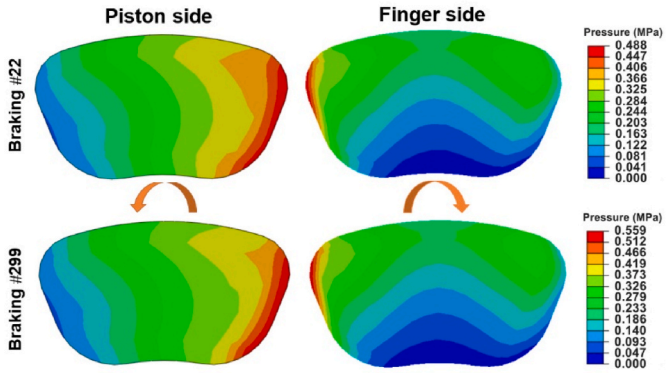

Fig. 8. Contact pressure contour plots of the piston and finger sides of braking events #22 and #299. Arrows indicate the rotating direction of the brake rotor.

From Fig. 8, the contact pressure distribution was observed to be different on the sides of piston and finger pads. Such a phenomenon could be possibly explained by the following factors: (1) the contact

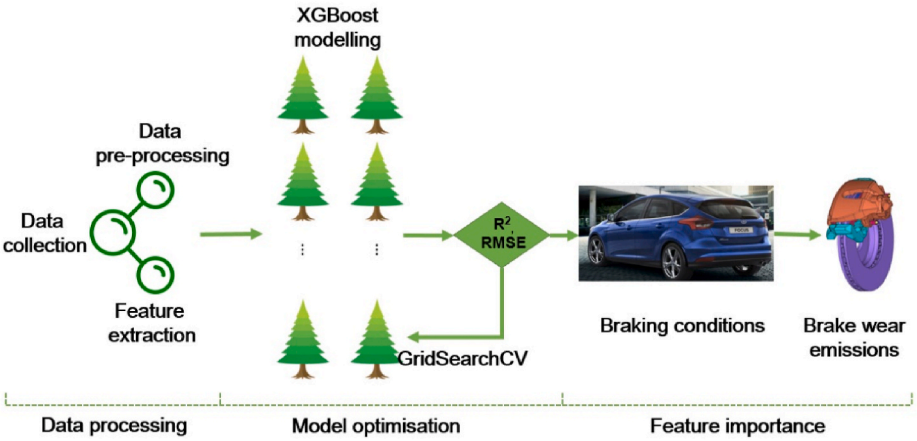

Fig. 7. The framework of the proposed methodology.

pressure applied to the piston side was different from the finger side because the load was applied in different ways where the piston pushed one pad into contact with the brake disc whereas the other was pushed into contact with the brake disc by reaction of the floating calliper; (2) the brake torque caused by the rotating disc might have an effect solely on the pad of piston side since the piston side pressure was a gradient in the tangential direction from outer to inner side; (3) due to the continual change in rotational velocity, no steady-state condition was attained at the end of every braking event. Thus, no uniform distribution of contact pressure was achieved. Similarly, Riva et al. (2020) used an FEA approach to observe that the contact pressure distributions acting on the pads of the piston and finger side were different. The same phenomenon was observed by AbuBakar and Ouyang (2008). In a study by Wahlström et al. (2009), however, their contour plots of contact pressure distribution were not the same as the results in our current work, which is probably attributed to the fact that the impact of the floating calliper on contact pressure was not considered in their study. The floating calliper would induce asymmetric effects between the pads of finger and piston side (Riva et al., 2019).

The piston and finger pad wear for braking events #22 and #299 are shown in Fig. 9. The pattern of contour plots regarding pad wear was similar for both braking events. Compared to the piston side pad, the finger side pad showed slightly less wear. The wear of both side pads showed a gradient increase from the inner to outer radii. The sliding distance on the external radii is always larger, which may explain why both side pads showed that the bigger the radius, the more wear could be caused. A similar view was reported by Riva et al. (2019), who simulated the brake pad wear using an FEA approach and found higher wear with larger radii. Valota et al. (2017) simulated the brake pad wear of the disc brake system with a fixed calliper in the SAE-J2707 cycle. It was found that the pad wear was more uniform, but was centred predominantly in the top portion of the contact region, which is not in line with our results. It is likely to be attributable to the fact that the contact pressure distribution was different when a fixed calliper was configured in the brake system since the braking mechanism was not the same. Mamakos et al. (2020) discovered that the measured PM for the brake system with a fixed calliper was up to 50% higher than that with a floating calliper during experimental tests on a brake dynamometer.

3.2. Measured and simulated PM_{10} emissions

Fig. 10 illustrates the simulated and measured PM_{10} emissions for each braking event of the WLTP-B cycle. The brake wear PM_{10} emissions were different for each of the 303 brake events due to the difference in braking conditions. Among 303 brake events, the worst brake event in terms of the measured and simulated PM_{10} was #295, which was from 133 km/h to 34 km/h with a deceleration of 1.82 m/s^2 and the longest sliding distance. In addition, most of the simulated PM_{10} emissions were lower than the measured ones. Such a phenomenon was probably ascribed to the following factors: the coefficient of friction between the brake disc and pad kept changing during the brake dynamometer tests, whereas the coefficient of friction in the FEA was set as constant; At a high initial velocity, the measured PM_{10} emissions are partially from the escaped particles due to brake drag (Hagino et al., 2016; Zum Hagen et al., 2019), whereas the FEA approach has no way to consider this effect of brake drag. Similarly, Riva et al. (2019) used an FEA approach to study the brake wear emissions in the Los Angeles city traffic cycle and found that the simulated results were lower than those from experimental ones.

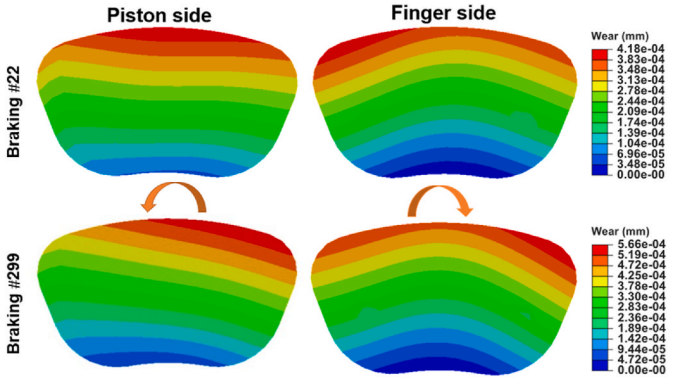

Fig. 9. Wear of the pads on the piston and finger side in the braking events #22 and #299. Arrows indicate the rotational direction of the brake rotor.

The total PM_{10} emissions for the measurement and simulation of each WLTP-B trip are summarised in Table 2. The simulation results showed that the total PM_{10} emissions were overestimated for trips 1, 6, and 9, whereas the PM_{10} emissions for other trips were underestimated. For each trip of the WLTP-B cycle, the relative error was all less than 20% between the measured and simulated results. The relative error of the total amount of PM_{10} emissions during the WLTP-B was 9%. In addition, total brake wear PM_{10} emissions during the WLTP-B cycle were 532.54 ± 24.43 mg using the gravimetric method, which was 12% higher than that using an FEA approach. Among these trips, PM_{10} emissions from the trip #10 were the largest contributor, accounting for 49% of the total PM_{10} emissions during the WLTP-B driving cycle. This may be attributed mainly to the following factors: (1) the trip #10 includes 114 braking events, accounting for 38% of the total braking events; (2) the majority of braking deceleration took place at high speeds, resulting in increased PM_{10} emissions.

To further assess the correlation between the measured and simulated results, the square correlation coefficient (R^2) and root mean square error (RMSE) were assessed, as shown in Fig. 11. The values of R^2 and RMSE were 0.93 and 0.018, respectively, which indicated that the measured results in the brake dynamometer tests had a strong correlation with the simulated results. Based on the current results, overall, the proposed approach for simulating brake wear PM_{10} emissions is promising. In the follow-up studies, the following aspects are required to be performed: (1) the simulation work for different brake systems will be performed to completely validate the model; (2) the brake wear $PM_{2.5}$ emissions will be predicted if a *pv*-map of the $PM_{2.5}$ mass rate is available and compared with measured results on a brake dynamometer; (3) the number concentrations of PM_{10}, $PM_{2.5}$, and even PM_1 will be evaluated on a brake dynamometer; (4) the particle number of brake wear will be explored using the proposed simulation approach if the *pv*-map is available for the particle number rate with varying contact pressure and sliding velocity. However, it is worth mentioning that the *pv*-map of particle number rates does not include volatile nanoparticles because if volatile nanoparticles are included, the measured results are difficult to repeat and reproduce.

The emission factors from simulated and measured PM_{10} emissions under the WLTP-B cycle were also calculated in the current work, as illustrated in Table 3. It was found that the emission factors of the brake system with low-metallic brake pad from a medium-sized passenger car during the WLTP-B cycle were 6.4 mg km^{-1} veh^{-1} and 7.0 mg km^{-1} veh^{-1}, respectively, in line with the data reported in most literature. For instance, Beddows and Harrison (2021) estimated the PM_{10} emission factor of brake wear using receptor modelling and reported that the mean PM_{10} emission factor from passenger cars on urban, rural and motorway roads was 6.2 mg km^{-1} veh^{-1}. Piscitello et al. (2021) used the same method to calculate the PM_{10} emission factor of 7.4 mg km^{-1} veh^{-1}. The same result (7.4 mg km^{-1} veh^{-1}) for the PM_{10} emission factor was reported by the European Environmental Agency (EEA, 2019). In a brake dynamometer study by Iijima et al. (2008) and Garg et al. (2000), they measured PM_{10} emission factors of 5.8 mg km^{-1} veh^{-1} and 5.2 mg km^{-1} veh^{-1}, respectively. However, Sanders et al. (2003) obtained a slightly higher PM_{10} emission factor of 8.1 mg km^{-1} veh^{-1} in a brake dynamometer test.

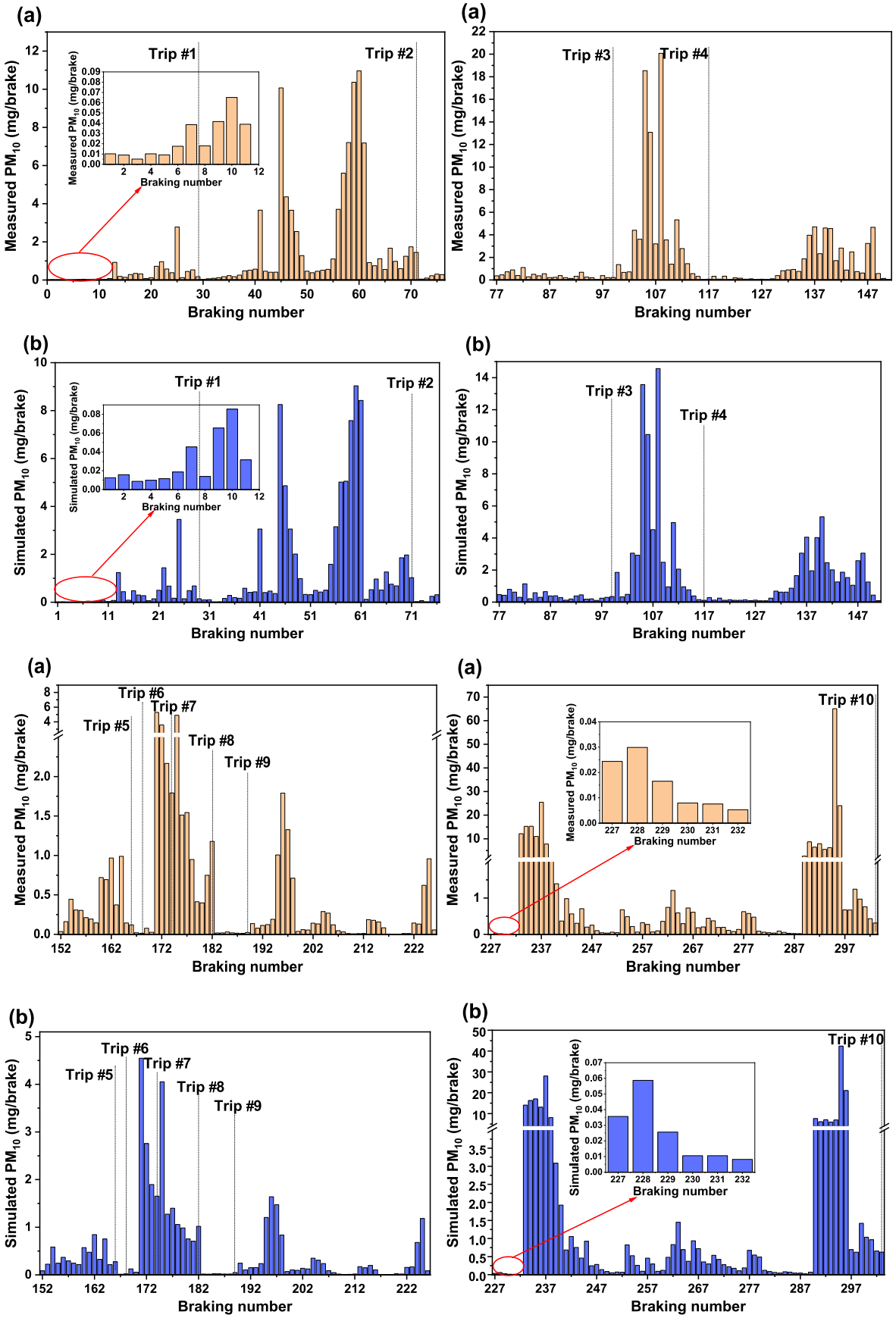

Fig. 10. Measured PM_{10} emissions (a) and simulated PM_{10} emissions (b) for brake events 1–303.

Table 2
Measured and simulated PM_{10} results of each trip of the WLTP-B cycle.

Trip number #	Measured PM_{10} (mg)	Simulated PM_{10} (mg)	Relative error
Trip #1	9.45 ± 1.42	11.14	−18%
Trip #2	89.09 ± 13.36	77.57	13%
Trip #3	10.09 ± 1.51	9.81	3%
Trip #4	81.15 ± 12.17	64.60	20%
Trip #5	51.09 ± 7.66	48.12	6%
Trip #6	0.03 ± 0.01	0.04	−7%
Trip #7	12.92 ± 0.65	11.04	15%
Trip #8	11.63 ± 1.74	11.25	3%
Trip #9	0.13 ± 0.02	0.16	−17%
Trip #10	245.78 ± 36.87	233.42	5%
Total	511.37 ± 76.71 (ELPI)	467.15	9%
	532.54 ± 24.43 (Gravimetric method	467.15	12%

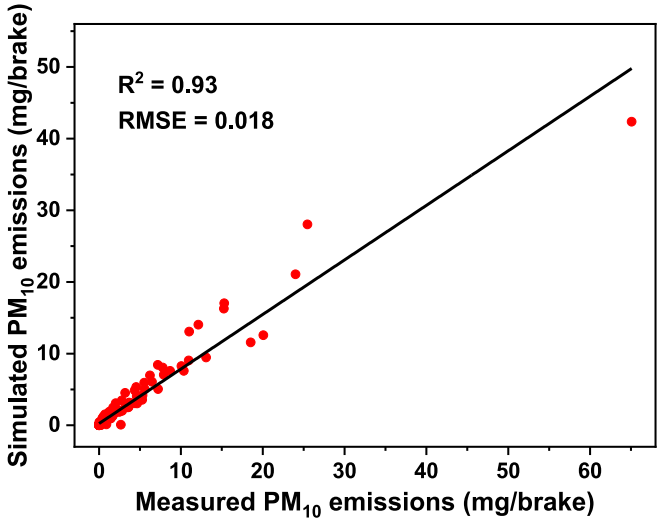

Fig. 11. Correlation between measured and simulated PM_{10} emissions.

Table 3
Summary of the PM_{10} emission factors (EFs) from brake wear.

Reference	Data sources	PM_{10} EFs (mg km^{-1} veh^{-1})
Present work	Simulation study	6.4
Present work	Brake dynamometer study	7.0
Beddows and Harrison (2021)	Receptor modelling	6.2
Piscitello et al. (2021)	Receptor modelling	7.4
(EEA, 2019)	Emission inventory	7.4
NAEI (2018)	Emission inventory	7.0
Timmers and Achten (2016)	Receptor modelling	9.3
Iijima et al. (2008)	Brake dynamometer study	5.8
Dahl et al. (2006)	Receptor modelling	7.4
Sanders et al. (2003)	Brake dynamometer study	8.1
Garg et al. (2000)	Brake dynamometer study	5.2

3.3. Effect of braking conditions on PM_{10} emissions

The XGBoost model was used to capture the non-linear correlations and explore the effect of braking conditions on brake wear PM_{10} emissions under the WLTP-B cycle. The measured 303 PM_{10} emissions and corresponding braking conditions were used as the analysis database. Similarly, two widely used evaluation indexes, R^2 and RMSE, were employed to evaluate the accuracy of the XGBoost model. The values of R^2 and RMSE were 0.94 and 0.009, respectively, which proves a strongly positive relationship between the optimised XGBoost model and experimental PM_{10} results. Thereafter, the XGboost was utilised to measure the feature importance regarding braking conditions.

According to the modelling results, the top five features that presented the highest importance on brake wear PM_{10} emissions are shown in Fig. 12. The total energy dissipated per stop showed the largest impact on brake wear PM_{10} emissions, followed by initial braking velocity, final rotor temperature, braking power, and deceleration rate. Initial braking velocity and deceleration rate can be classified as control parameters of braking conditions as they can be governed by the driver; final rotor temperature belongs to the response parameter; braking power and total dissipation energy are derivative parameters as they are highly dependent upon braking conditions. Previous studies have revealed that these parameters associated with braking conditions are closely related to brake wear emissions, but the importance ranking of these parameters has not been determined. For instance, Vojtisek-Lom et al. (2021) investigated the impact of braking conditions on brake wear particles of passenger cars on a brake dynamometer and found that these particles strongly depended on the combined effects of rotor temperature, braking power, and total energy dissipated. Zum Hagen et al. (2019) reported that the BWP mass presented an exponential proportion to the total dissipation energy during the stop. The brake wear emissions during various test driving cycles were conducted by Woo et al. (2021), who found that the brake wear emissions for each test driving cycle were proportional to the brake energy dissipated and initial velocity. Park et al. (2021) revealed that more brake wear particles were emitted at higher velocity braking applications since the braking at higher velocity generally corresponded to more energy dissipation. In a study by Grigoratos and Martini (2015), high temperatures at the interface between brake pads and rotor were found to cause the decomposition of brake lining materials, which would promote the generation of ultrafine particles. The same conclusion was reached by Perricone et al. (2019). Nosko et al. (2015) performed an experimental analysis and confirmed that temperature was a major factor affecting airborne PM of brake wear. In addition, brake temperature exerted a substantial influence on brake particle number concentrations, particularly at temperatures higher than the critical temperature (Alemani, 2017; Alemani et al., 2017; Mathissen et al., 2011, 2018). Limiting harsh and extreme braking events would thus effectively mitigate the brake wear emissions. In terms of brake deceleration rate, many studies have identified the significant impact on brake wear emissions (Hagino et al., 2016; Kwak et al., 2013; Mathissen et al., 2011; Oroumiyeh and Zhu, 2021; Thorpe

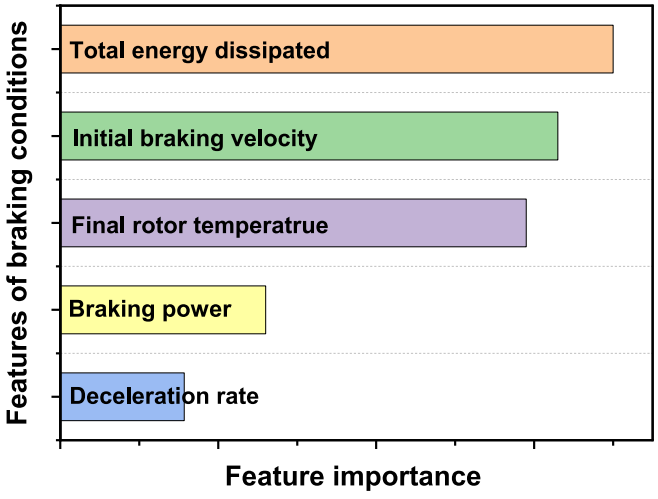

Fig. 12. Feature importance ranking based on XGBoost outputs.

and Harrison, 2008). To the best of the authors' knowledge, no research was reported regarding the importance rankings of these factors that contribute to the brake wear PM_{10} emissions. It is, however, worth mentioning that even though the XGBoost model can evaluate the importance ranking of braking conditions affecting brake wear PM_{10} emissions, it remains unclear how each variable of braking conditions quantitatively determines output results. In our follow-up work, it is required to quantitatively identify relationships between braking conditions and brake wear emissions.

In addition, previous studies have demonstrated the effects of vehicle types on brake wear emissions. For instance, Garg et al. (2000) revealed that brake wear particles from large pickup trucks were more than twice that of small cars. In addition, they found that the total suspension particles, $PM_{2.5}$ and PM_{10} from larger passenger cars were 55% more than those from small passenger cars. The U.S. Environmental Protection Agency (EPA, 2014) distinguished brake wear $PM_{2.5}$ and PM_{10} emission factors from passenger cars and passenger trucks and reported that the latter emitted 67% more PM_{10} and $PM_{2.5}$ brake wear emissions. The European Environment Agency (EEA) published an emission inventory guidebook (Ntziachristos and Boulter, 2013). It was found that the emissions factors of PM_{10} and $PM_{2.5}$ from light-duty vehicles were 57% higher than those from passenger cars.

4. Conclusions

This work focuses on the brake wear particle emissions of a medium-sized passenger vehicle under the WLTP-B cycle using FEA and experimental approaches. Moreover, a machine learning method (i.e. XGBoost) was employed to capture the importance rankings of braking conditions contributing to PM_{10} emissions from brake wear. The FEA results showed that the contact pressure on the piston side showed a transversal increase from outer to inner side, whilst the contact pressure on the finger side increased gradiently from small to large radii. The brake pad wear depth presented a gradient increase from small to large radii. In addition, the simulated and measured PM_{10} results showed good agreement overall, with a relative error of 9% and 12%, respectively, although the simulated results were underestimated relative to the measured ones. It means that the proposed simulation approach appears to be capable of computing brake wear PM_{10} emissions under the WLTP-B cycle. The simulated and experimental PM_{10} emission factors were 6.4 mg km^{-1} veh^{-1} and 7.0 mg km^{-1} veh^{-1} during the WLTP-B cycle, respectively. Among the 10 trips of this cycle, trip #10 contributed up to 49% of the total PM_{10} emissions. Furthermore, the XGBoost results indicated the top five most important parameters affecting the brake wear PM_{10} emissions, which were the dissipation energy, initial braking speed, final rotor temperature, braking power, and deceleration rate. From friendly driving behaviour and regulation perspective, limiting severe braking and high-speed braking has the potential to reduce PM_{10} emissions from brake wear.

CRediT authorship contribution statement

Ye Liu: Investigation, Methodology, Data visualisation, Writing – original draft. **Sijin Wu:** Software, Formal analysis, Writing – review & editing. **Haibo Chen:** ConceptualizationConceptualisation, Funding acquisition, Project administration. **Matteo Federici:** Resources, Data curation, Writing – review & editing. **Guido Perricone:** Resources, Data curation. **Ying Li:** Methodology, Writing – review & editing. **Gang Lv:** Software, Data curation, Writing – review & editing. **Said Munir:** Writing – review & editing. **Zhiwen Luo:** Writing – review & editing. **Baohua Mao:** Writing – review & editing.

Declaration of competing interest

The authors declare that they have no known competing financial interests or personal relationships that could have appeared to influence the work reported in this paper.

Acknowledgments

This research was jointly supported by the European Union's Horizon 2020 research and innovation programme: MODALES (grant agreement No 815189, https://modales-project.eu/) aimed at modifying drivers' behaviour to reduce vehicle emissions from brake wear, and nPETS (grant agreement No 954377, https://www.npets-project.eu/) aimed at studying the life of the sub 100 nm particles emitted from transport from their creation to their potential path to human beings and animals and the Natural Science Foundation of Tianjin (19JCZDJC40100).

Appendix A. Supplementary data

Supplementary data to this article can be found online at https://doi.org/10.1016/j.jclepro.2022.132278.

References

Abaqus. Information of abaqus ALE technique. available at: http://abaqus.software.polimi.it/v6.14/books/usi/default.htm?startat=pt03ch14s06.html.
AbuBakar, A.R., Ouyang, H., 2008. Wear prediction of friction material and brake squeal using the finite element method. Wear 264 (11–12), 1069–1076.
Ahmad, G.N., Fatima, H., Saidi, A.S., 2022. Efficient Medical Diagnosis of Human Heart Diseases Using Machine Learning Techniques with and without GridSearchCV. IEEE Access.
Alemani, M., 2017. Particle Emissions from Car Brakes: the Influence of Contact Conditions on the Pad-To-Rotor Interface. KTH Royal Institute of Technology.
Alemani, M., Gialanella, S., Straffelini, G., Ciudin, R., Olofsson, U., Perricone, G., Metinoz, I., 2017. Dry sliding of a low steel friction material against cast iron at different loads: characterization of the friction layer and wear debris. Wear 376–377, 1450–1459.
Amato, F., 2018. Non-exhaust Emissions: an Urban Air Quality Problem for Public Health; Impact and Mitigation Measures. Academic Press.
Amato, F., Cassee, F.R., Denier van der Gon, H.A.C., Gehrig, R., Gustafsson, M., Hafner, W., Harrison, R.M., Jozwicka, M., Kelly, F.J., Moreno, T., Prevot, A.S.H., Schaap, M., Sunyer, J., Querol, X., 2014. Urban air quality: the challenge of traffic non-exhaust emissions. J. Hazard Mater. 275, 31–36.
Beddows, D.C.S., Harrison, R.M., 2021. PM10 and PM2.5 emission factors for non-exhaust particles from road vehicles: dependence upon vehicle mass and implications for battery electric vehicles. Atmos. Environ. 244, 117886.
Chen, J., Li, W., Zhang, H., Jiang, W., Li, W., Sui, Y., Song, X., Shibasaki, R., 2020. Mining urban sustainable performance: GPS data-based spatio-temporal analysis on on-road braking emission. J. Clean. Prod. 270, 122489.
Dahl, A., Gharibi, A., Swietlicki, E., Gudmundsson, A., Bohgard, M., Ljungman, A., Blomqvist, G., Gustafsson, M., 2006. Traffic-generated emissions of ultrafine particles from pavement–tire interface. Atmos. Environ. 40 (7), 1314–1323.
EEA, 2018. European Union Emission Inventory Report 1990-2016 under the UNECE Convention on Long-Range Transboundary Air Pollution (LRTAP). EEA Report.
EEA, 2019. Airbase - the European Air Quality Database. European Environment Agency.
Environmental Protection Agency, 2014. Brake and Tire Wear Emissions from On-Road Vehicles in MOVES2014. Environmental Protection Agency (EPA), Washington DC, USA.
Fan, Y.V., Perry, S., Klemeš, J.J., Lee, C.T., 2018. A review on air emissions assessment: Transportation. J. Clean. Prod. 194, 673–684.
Garg, B.D., Cadle, S.H., Mulawa, P.A., Groblicki, P.J., Laroo, C., Parr, G.A., 2000. Brake wear particulate matter emissions. Environ. Sci. Technol. 34 (21), 4463–4469.
Gasser, M., Riediker, M., Mueller, L., Perrenoud, A., Blank, F., Gehr, P., Rothen-Rutishauser, B., 2009. Toxic effects of brake wear particles on epithelial lung cells in vitro. Part. Fibre Toxicol. 6 (1), 1–13.
Grigoratos, T., Martini, G., 2015. Brake wear particle emissions: a review. Environ. Sci. Pollut. Control Ser. 22 (4), 2491–2504.
Hagino, H., Oyama, M., Sasaki, S., 2016. Laboratory testing of airborne brake wear particle emissions using a dynamometer system under urban city driving cycles. Atmos. Environ. 131, 269–278.
Harrison, R.M., Jones, A.M., Gietl, J., Yin, J., Green, D.C., 2012. Estimation of the contributions of brake dust, tire wear, and resuspension to nonexhaust traffic particles derived from atmospheric measurements. Environ. Sci. Technol. 46 (12), 6523–6529.
Iijima, A., Sato, K., Yano, K., Kato, M., Kozawa, K., Furuta, N., technology, 2008. Emission factor for antimony in brake abrasion dusts as one of the major atmospheric antimony sources. Environ. Sci. Technol. 42 (8), 2937–2942.
Kim, K.-H., Kabir, E., Kabir, S., 2015. A review on the human health impact of airborne particulate matter. Environ. Int. 74, 136–143.
Kwak, J.H., Kim, H., Lee, J., Lee, S., 2013. Characterization of non-exhaust coarse and fine particles from on-road driving and laboratory measurements. Sci. Total Environ. 458, 273–282.

Lawrence, S., Sokhi, R., Ravindra, K., Mao, H., Prain, H.D., Bull, I.D., 2013. Source apportionment of traffic emissions of particulate matter using tunnel measurements. Atmos. Environ. 77, 548–557.
Liu, Y., Chen, H., Gao, J., Li, Y., Dave, K., Chen, J., Federici, M., Perricone, G., 2021. Comparative analysis of non-exhaust airborne particles from electric and internal combustion engine vehicles. J. Hazard Mater. 420, 126626.
Liu, Y., Chen, H., Li, Y., Gao, J., Dave, K., Chen, J., Li, T., Tu, R., 2022. Exhaust and non-exhaust emissions from conventional and electric vehicles: a comparison of monetary impact values. J. Clean. Prod. 331, 129965.
Mamakos, A., Arndt, M., Hesse, D., Hamatschek, C., Augsburg, K., 2020. Comparison of Particulate Matter and Number Emissions from a Floating and a Fixed Caliper Brake System of the Same Lining Formulation. SAE Technical Paper Series.
Mathissen, M., Grochowicz, J., Schmidt, C., Vogt, R., Farwick zum Hagen, F.H., Grabiec, T., Steven, H., Grigoratos, T., 2018. A novel real-world braking cycle for studying brake wear particle emissions. Wear 414–415, 219–226.
Mathissen, M., Scheer, V., Vogt, R., Benter, T., 2011. Investigation on the potential generation of ultrafine particles from the tire–road interface. Atmos. Environ. 45 (34), 6172–6179.
NAEI, 2018. Road transport emission factor from NAEI 2018. https://naei.beis.gov.uk/data/ef-transport.
Nosko, O., Alemani, M., Olofsson, U., 2015. Temperature Effect on Emission of Airborne Wear Particles from Car Brakes. Europe's Braking Conference and Exhibition, pp. 4–6.
Ntziachristos, L., Boulter, P., 2013. Road Vehicle Tyre and Brake Wear. Road Surface Wear. European Environment Agency, Copenhagen.
OECD, 2020. Non-exhaust Particulate Emissions from Road Transport: an Ignored Environmental Policy Challenge. OECD Publishing, Paris. https://doi.org/10.1787/4a4dc6ca-en.
Oroumiyeh, F., Zhu, Y., 2021. Brake and Tire Particles Measured from On-Road Vehicles: Effects of Vehicle Mass and Braking Intensity. Atmospheric Environment, p. 12.
Park, J., Joo, B., Seo, H., Song, W., Lee, J.J., Lee, W.K., Jang, H., 2021. Analysis of Wear Induced Particle Emissions from Brake Pads during the Worldwide Harmonized Light Vehicles Test Procedure (WLTP, pp. 466–467.
Pedregosa, F., Varoquaux, G., Gramfort, A., Michel, V., Thirion, B., Grisel, O., Blondel, M., Prettenhofer, P., Weiss, R., Dubourg, V., 2011. Scikit-learn: machine learning in Python. J. Mach. Learn. Res. 12, 2825–2830.
Perricone, G., Alemani, M., Wahlström, J., Olofsson, U., 2019. A proposed driving cycle for brake emissions investigation for test stand. Proc. Inst. Mech. Eng. - Part D J. Automob. Eng. 234 (1), 122–135.
Piscitello, A., Bianco, C., Casasso, A., Sethi, R., 2021. Non-exhaust traffic emissions: sources, characterization, and mitigation measures. Sci. Total Environ. 766, 144440.
Riva, G., Valota, G., Perricone, G., Wahlström, J., 2019. An FEA approach to simulate disc brake wear and airborne particle emissions. Tribol. Int. 138, 90–98.
Riva, G., Varriale, F., Wahlström, J., 2020. A finite element analysis (FEA) approach to simulate the coefficient of friction of a brake system starting from material friction characterization. Friction 9 (1), 191–200.
Riva, G., Wahlström, J., Alemani, M., Olofsson, U., 2017. A CFD Study of a Pin-On-Disc Tribometer Setup Focusing on Airborne Particle Sampling Efficiency, ECOTRIB 2017, 6th European Conference on TRIBology 7–9 June 2017, Ljubljana, Slovenia.
Rodovalho, E.d.C., de Tomi, G., 2017. Reducing environmental impacts via improved tyre wear management. J. Clean. Prod. 141, 1419–1427.
Sanders, P.G., Xu, N., Dalka, T.M., Maricq, M.M., 2003. Airborne brake wear debris: size distributions, composition, and a comparison of dynamometer and vehicle tests. Environ. Sci. Technol. 37 (18), 4060–4069.
Thorpe, A., Harrison, R.M., 2008. Sources and properties of non-exhaust particulate matter from road traffic: a review. Sci. Total Environ. 400 (1–3), 270–282.
Timmers, V.R.J.H., Achten, P.A.J., 2016. Non-exhaust PM emissions from electric vehicles. Atmos. Environ. 134, 10–17.
Valota, G., De Luca, S., Söderberg, A., 2017. Using a Finite Element Analysis to Simulate the Wear in Disc Brakes during a Dyno Bench Test Cycle. Proceedings of the Eurobrake, Dresden, Germany, pp. 2–4.
Vojtisek-Lom, M., Vaculik, M., Pechout, M., Hopan, F., Arul Raj, A.F., Penumarti, S., Horak, J.S., Popovicheva, O., Ondracek, J., Dousova, B., 2021. Effects of braking conditions on nanoparticle emissions from passenger car friction brakes. Sci. Total Environ. 788, 147779.
Wahlström, J., Matejka, V., Lyu, Y., Söderberg, A., 2017. Contact pressure and sliding velocity maps of the friction, wear and emission from a low-metallic/cast-Iron disc brake contact pair. Tribology in Industry 39 (4), 460–470.
Wahlström, J., Söderberg, A., Olofsson, U., 2009. Simulation of Airborne Wear Particles from Disc Brakes. SAE Technical Paper.
Woo, S.-H., Kim, Y., Lee, S., Choi, Y., Lee, S., 2021. Characteristics of Brake Wear Particle (BWP) Emissions under Various Test Driving Cycles. Wear, pp. 480–481.
Xu, J., Wang, A., Schmidt, N., Adams, M., Hatzopoulou, M., 2020. A gradient boost approach for predicting near-road ultrafine particle concentrations using detailed traffic characterization. Environ. Pollut. 265, 114777.
Zum Hagen, F.H.F., Mathissen, M., Grabiec, T., Hennicke, T., Rettig, M., Grochowicz, J., Vogt, R., Benter, T., 2019. Study of brake wear particle emissions: impact of braking and cruising conditions. Environ. Sci. Technol. 53 (9), 5143–5150.